12-21-2012

Facile Molten-Salt Synthesis of Double Perovskite La2BMnO 6 Nanoparticles

Yuanbing Mao
The University of Texas Rio Grande Valley, yuanbing.mao@utrgv.edu

RSC Advances

Cite this: *RSC Advances*, 2012, **2**, 12675–12678

www.rsc.org/advances

COMMUNICATION

Facile molten-salt synthesis of double perovskite La_2BMnO_6 nanoparticles†

Yuanbing Mao*

Received 13th August 2012, Accepted 16th October 2012
DOI: 10.1039/c2ra21789a

Crystalline double perovskite La_2BMnO_6 (B = Ni and Co) nanoparticles with an average grain size of ~64 nm were successfully prepared using a facile, environmentally friendly, scalable molten-salt reaction at 700 °C in air. Their composition and structural and magnetic properties have been characterized.

Multifunctional materials show various responses to multiple external stimuli enabling novel device applications including intelligent sensors, spintronics, solid-state thermoelectric coolers, and other functional devices. For example, double perovskite oxides with general formula $AA'BB'O_6$, where A/A′ = rare earth or alkaline earth metals and B/B′ = 3*d* transition metals, display a wide variety of interesting physical properties with composition variations. Considerable research activity is being carried out to explore new double perovskite materials, to understand the origin of their properties (*e.g.* magnetodielectric, magnetoresistance, magnetocapacitance), to improve their properties, and to adapt their materials chemistry to the production technology for each application.[1–7]

One of them, La_2NiMnO_6 (LNMO) has gained more attention as a rare example of a single-material platform with multiple functions, such as magnetocapacitance and magnetoresistance effects. Due to its spin lattice coupling, and also a large magnetodielectric (MD) effect close to room temperature, it has been demonstrated that the spins, electric charge and dielectric functions in LNMO can be tuned by magnetic and/or electric fields.[1–6] It has also been confirmed that LNMO is a ferromagnetic (FM) semiconductor that has a Curie temperature (T_C) very close to room temperature with ordered Ni^{2+} and Mn^{4+} ions occupying the centers of corner-sharing BO_6 and $B'O_6$ in the structure, respectively, which is distorted from the ideal double perovskite. This conclusion is consistent with the Mn NMR and X-ray absorption spectroscopy results.[8,9] In some neutron and X-ray diffraction studies, bulk LNMO provided evidence for long-range ordering of Ni and Mn cations, even though different neutron-diffraction studies disagree on whether the oxidation states are Ni^{2+}/Mn^{4+} or Ni^{3+}/Mn^{3+}.[1,10] The isostructural system of LNMO, La_2CoMnO_6 (LCMO), possesses a ferromagnetic Curie transition temperature (FM-T_C) ~225 K with an insulating behavior.[3,7] Similar to those of the LNMO system, several reports have also shown that the magnetic properties of the LCMO system are related to cation ordering, which in turn depends on the synthesis conditions.[3,7,11–15] For instance, as reported in the literature, they can exhibit one or more magnetic transitions.[3,11,16,17] LNMO synthesized under some conditions would show two unobscured FM transitions which occur at about 150 and 280 K, respectively, with decreasing temperature.[3,16] An ordered sublattice with high spin Co^{2+} and Mn^{4+} pair in LCMO gives a FM transition ~220 K, while a disordered sublattice with low spin Co^{3+} and high spin Mn^{3+} invokes a FM transition below 150 K. It was also reported that in the case of low-temperature-sintered LCMO samples high T_C (~220 K) was observed, while the samples prepared at high temperature exhibited low T_C (~150 K). In ordered LCMO thin films, the observed MD effect near T_C was attributed to spin–lattice coupling. On the other hand, 0.8% of MD response was observed at 280 K in polycrystalline LCMO system.[17] Raman measurements showed a spin–lattice coupling near the two magnetic transitions in LCMO bulk.[11]

Recently, nanostructures (*e.g.*, nanoparticles, nanowires, and nanotubes) made of metal oxides, metals and carbon have been investigated as emerging materials because they exhibit interesting physical properties, which are different from those of their bulk and thin film counterparts.[18–21] In the case of double perovskite oxides, the majority of the previous work has focused on $AA'BB'O_6$ single crystals and thin films.[1–17] However, it can be concluded that the discrepancies mentioned above in the studies of both LNMO and LCMO samples originate from the different synthetic procedures and conditions employed. So far, there are very few reports on LNMO and LCMO nanostructures. The only reported synthetic method for LNMO and LCMO nanoparticles is based on a sol–gel process.[2] In this work, we employed a facile and scalable molten-salt synthesis process to prepare crystalline LNMO and LCMO nanoparticles in a mixing salt medium, *i.e.* $NaNO_3$ and KNO_3 (1 : 1), at 700 °C.[22,23] To the best of our knowledge, we are the first to report the successful synthesis of pure LNMO and LCMO nanoparticles *via* a molten-salt synthesis. The intrinsic simplicity, flexibility and scalability of the molten-salt synthesis render it attractive for the preparation of a wide range of double perovskite $AA'BB'O_6$ nanomaterials. It also provides a starting point for further study of the synthesis–structure-property relationships of a wide range of double perovskite $AA'BB'O_6$ nanomaterials.

Powder XRD was used to characterize the as-synthesized LNMO and LCMO nanoparticles. As shown in Fig. 1, no extra reflection

Department of Chemistry, University of Texas – Pan American, Edinburg, TX 78539 USA. E-mail: maoy@utpa.edu.; Fax: +1 956 665 5006; Tel: +1 956 665 2417

† Electronic supplementary information (ESI) available: Enlarged HRTEM images as shown in Fig. 4. See DOI: 10.1039/c2ra21789a

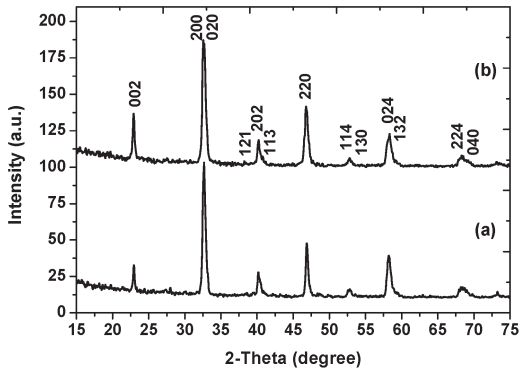

Fig. 1 XRD patterns of the as-synthesized (a) LNMO and (b) LCMO nanoparticles.

peaks other than those of pure perovskite phase are observed within the experimental limit, which confirms the formation of single phase composition of LNMO and LCMO double perovskites.[2] Based on the Sherrer equation, the calculated crystalline domain sizes are 26 nm for LNMO and 20 nm for LCMO, which are 2–3 times smaller than the particle/grain sizes measured by TEM as shown below.

Raman spectroscopy is an excellent tool to obtain useful information on the local structure of the different microphases or macrophases present simultaneously in many manganites. Fig. 2 shows the Raman spectrum obtained from the LNMO nanoparticles. The spectrum is dominated by two broad peaks at around 524 and 670 cm^{-1}, which can be assigned to the A_g antisymmetric stretching (or Jahn–Teller stretching mode) and B_g symmetric stretching vibrations of the MnO_6 octahedra, respectively. A noticeable difference is seen between our LNMO nanoparticles and the bulk sample: the A_g and B_g peaks for the nanoparticles shift to higher energy, 3 and 9 cm^{-1}, respectively, when compared to the bulk crystal. The peak shifts occur due to surface strain from the nanosized particles.[24]

Typical SEM images of the as-synthesized LNMO and LCMO nanoparticles are shown in Fig. 3. These nanostructures, prepared at temperature of 700 °C by the facile molten-salt synthesis, are spherical and relatively quite uniform. Even though it is difficult to determine their exact size at this magnification, it is determined by TEM in the following paragraph.

Fig. 4(a) and 4(c) show general low-magnification TEM images of LNMO and LCMO nanoparticles, respectively. These images demonstrated that LNMO and LCMO nanoparticles with particle/grain sizes of 65 ± 18 nm and 58 ± 20 nm (based on 45 particles each), respectively, were prepared by the molten-salt synthetic procedure at a temperature of 700 °C. They are not always spherical,

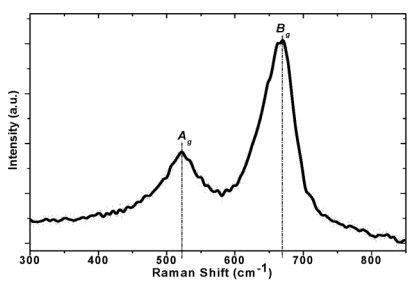

Fig. 2 Raman spectrum of the as-synthesized LNMO nanoparticles.

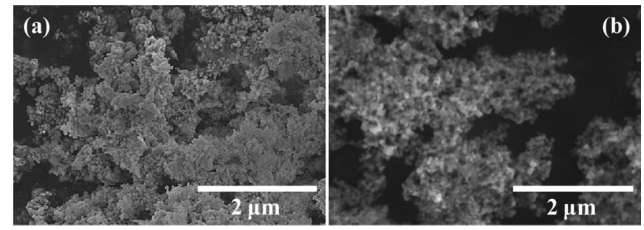

Fig. 3 SEM images of the as-synthesized (a) LNMO and (b) LCMO nanoparticles.

and some of them have clear edges. It is also easy to tell that our as-synthesized LNMO and LCMO nanoparticles are well dispersible, unlike those prepared by the sol–gel method. In our synthetic process, the molten salt mixture used acts as a separator between the formed nanoparticles or surfactant on the nanoparticles' surface. It prevents them from agglomerating during the nanoparticle growth process, and even during the cooling process. Fig. 4(b) and 4(d) and S1 (ESI†) show HRTEM images of LNMO and LCMO nanoparticles, respectively. These lattice images of individual nanoparticles show that they are crystalline. A high-resolution TEM image obtained from an individual LNMO nanoparticle (Fig. 4(b)) shows a typical crystalline domain with an interplanar spacing of about 2.65 Å, comparable to the {200} plane of a LNMO crystal. The corresponding energy dispersive X-ray spectrometry spectrum was taken and the elemental signatures of La, Ni and Mn metals are present. The selected-area electron diffraction data taken from the same individual LNMO nanoparticle (inset of Fig. 4(b)) shows sharp diffraction spots indicating the formation of well-developed and crystalline LNMO nanocrystals. Meanwhile, in Fig. 4(d), a high-resolution TEM image obtained from an individual LCMO nanoparticle shows a typical crystalline domain with an interplanar spacing of about 2.63 Å and 3.72 Å, comparable to the {200} and {002} planes of a LCMO crystal. The corresponding

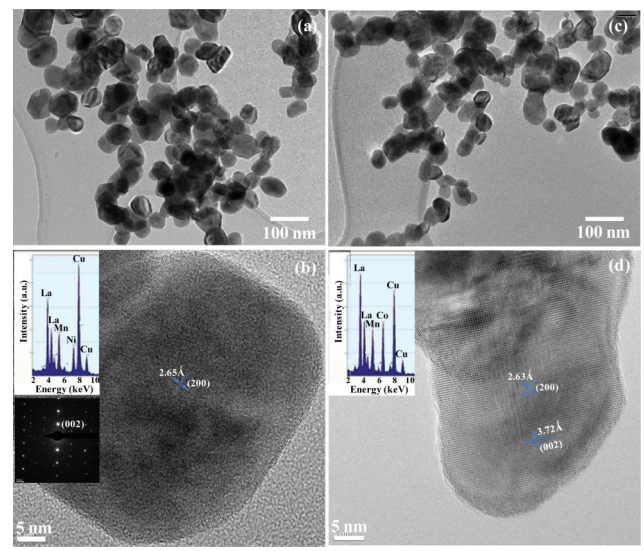

Fig. 4 Typical low magnification TEM images of the as-synthesized (a) LNMO and (c) LCMO nanoparticles. HRTEM images of the (b) LNMO and (d) LCMO nanoparticles with corresponding EDX (the Cu peaks originate from the TEM grid) as well as SAED of LNMO.

energy dispersive X-ray spectrometry spectrum was taken and the elemental signatures of La, Co and Mn metals are present.

Similarly to the previously reported synthesis of single perovskites,[23] the following reactions summarize a postulated reasonable mechanism for the synthesis of double perovskite La_2BMnO_6 (B = Ni and Co) nanocrystals:

$$La(NO_3)_3 + B(NO_3)_2 + Mn(NO_3)_4 \rightarrow La_2O_3 + BO + MnO_2$$

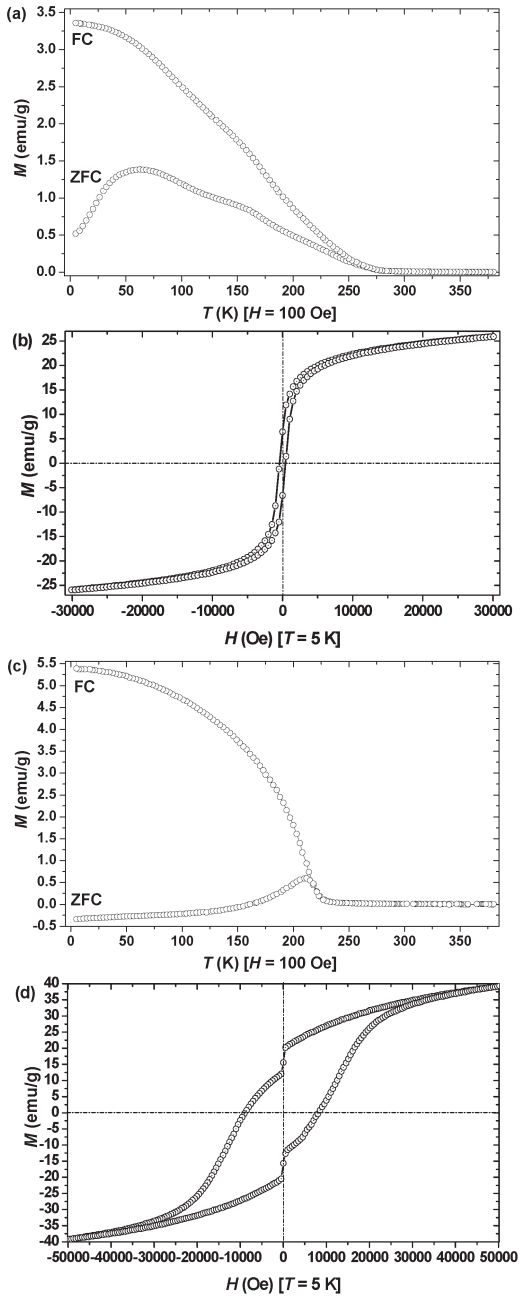

Fig. 5 (a) Temperature dependences of zero-field-cooled and field-cooled magnetization of LNMO nanoparticles in an applied field of 100 Oe. (b) Field-dependent magnetization data at 5 K of LNMO nanoparticles. (c) Temperature dependences of zero-field-cooled and field-cooled magnetization of LCMO nanoparticles in an applied field of 100 Oe. (d) Field-dependent magnetization data at 5 K of LCMO nanoparticles.

$$La_2O_3 + BO + MnO_2 \rightarrow La_2BMnO_6$$

Due to the differences of ionic radius and charge number (La^{3+}: 1.06 Å, Ni^{2+}: 0.69 Å, Co^{2+}: 0.72 Å, Mn^{4+}: 0.60 Å, Na^{+}: 0.97 Å, and K^{+}: 1.33 Å),[25] Na^{+} and K^{+} cannot be incorporated into the perovskite structure during our synthesis.

The temperature dependences of zero-field-cooled and field-cooled magnetization of the as-synthesized LNMO nanoparticles were measured from 5 to 380 K in a 100 Oe magnetic field and are shown in Fig. 5(a). Below 225 K, divergence has been observed between ZFC and FC magnetization curves. The FC magnetization reaches a maximum value of $\sim$3.4 emu g^{-1} at 5 K. The magnetic transition at $\sim$265 K indicates the onset of FE long-range ordering, very close to the magnetic transition temperature (T_C = $\sim$280 K) reported previously in the literature.[1] The difference may be attributed to the surface strain effects due to the nanoscale size of these nanoparticles, agreeing with the Raman spectrum in Fig. 2.[24] From the ZFC curve, a relative well-defined cusp can be observed at a temperature of 62.5 K, which may be defined as the freezing temperature T_P of magnetic clusters.[2] Fig. 5(b) shows the magnetization *versus* field (*M–H*) curves of LNMO nanoparticles. A hysteresis loop has been observed at 5 K with a coercive field of $\sim$500 Oe and remnant magnetization of $\sim$6 emu g^{-1}. Meanwhile, the temperature dependences of zero-field-cooled and field-cooled magnetization were measured for the as-synthesized LCMO nanoparticles from 5 to 380 K in a 100 Oe magnetic field (Fig. 5(c)). Below 210 K, divergence has been observed between ZFC and FC magnetization curves, similar to the difference in low-field ZFC and FC magnetization data measured from LNMO nanoparticles. These LCMO nanoparticles possess a single magnetic transition at about 235 K under 100 Oe field, which is very close to the magnetic transition temperature reported previously for the well-ordered bulk LCMO.[7] The FC magnetization reaches a maximum value of $\sim$5.4 emu g^{-1} at 5 K. Fig. 5(d) shows the magnetization *versus* field (*M–H*) curves of LCMO nanoparticles. A hysteresis loop has been observed at 5 K with a coercive field of $\sim$8.5 kOe and remnant magnetization of $\sim$20 emu g^{-1}, and both are much larger than those measured from the as-synthesized LNMO nanoparticles as shown in Fig. 5(b). Aside from the magnetic properties presented here, detailed investigation is underway and extensive results will be reported elsewhere shortly.

Conclusions

In summary, nanocrystals with double perovskite structure, La_2BMnO_6 (B = Ni and Co) composition and an average grain size of $\sim$64 nm have been successfully synthesized by a simple, scalable, and efficient molten-salt synthetic process using metallic nitrates as precursors. This strategy is attractive for the preparation of a wide range of other complex double and even triple perovskite nanocrystals. Moreover, the magnetic properties of these double perovskite nanocrystals indicate that these nanoparticles are promising candidates for many applications such as intelligent sensors, spintronics, solid-state thermoelectric coolers, and other functional devices.

Experimental

In a typical sample preparation protocol of La_2BMnO_6 (B = Ni or Co in this study) nanocrystals, high-purity lanthanum nitrate, nickel

or cobalt nitrate, manganese nitrate, sodium nitrate, and potassium nitrate were mixed in a molar ratio of 2 : 1 : 1 : 60 : 60 and ground for 30 min with assistance of ethanol. The mixture was then placed within a covered nickel crucible, which was subsequently placed inside a box furnace and heated to 700 °C at a ramp rate of 2 °C min^{-1}. After isothermal annealing at 700 °C for 6 h, the resulting mixture was cooled to room temperature at a ramp rate of 5 °C min^{-1}. The resulting sample was subsequently purified with copious amounts of distilled water followed by centrifugation. The remaining precipitate was heated at 80 °C overnight in a drying oven.

For powder XRD analysis, the as-prepared samples of La_2BMnO_6 nanocrystals, after centrifugation, were subsequently sonicated for about 1 min and later air-dried upon deposition onto glass slides. Diffraction patterns of these materials were collected using a PANalytical X-ray diffractometer, operating in the Bragg configuration using Cu-Kα radiation (λ = 1.54 Å) from 15 to 75° at a scanning rate of 0.2° min^{-1}. The size and morphology of La_2BMnO_6 nanocrystals were characterized using a field emission scanning electron microscope (FESEM, FEI) at an accelerating voltage of 10 kV. Specifically, the as-prepared samples of La_2BMnO_6 nanocrystals, after centrifugation, were sonicated for about 1 min and later air-dried upon deposition onto clean silicon wafers, which were then attached onto the surfaces of SEM brass stubs. Transmission electron microscopy (TEM) images were obtained using a Philips CM-200 with a LaB_6 filament operated at an accelerating voltage of 200 kV. High-resolution TEM (HRTEM) images, selected-area electron diffraction (SAED) patterns and energy-dispersive X-ray spectroscopy (EDS) data were carried out on an FEI Tecnai F30 microscope at an accelerating voltage of 300 kV with a point-to-point resolution of 0.2 nm. Specimens for the TEM studies were prepared by sonicating aqueous suspension containing La_2BMnO_6 nanocrystals, followed by depositing a drop of the suspension of La_2BMnO_6 nanoparticles onto a 300 mesh Cu grid, coated with a lacey carbon film. The magnetic measurements were carried out in a 9-T physical properties measurement system (PPMS, Quantum Design).

Acknowledgements

The author acknowledges the University of Texas – Pan American for the startup support, Dr J. Huang at the Center for Integrated Nanotechnologies (CINT) of Sandia National Laboratories for TEM work, and J. Doyle and Dr R. Seshadri at the University of California, Santa Barbara, for magnetic measurements. The CINT, a U.S. Department of Energy, Office of Basic Energy Sciences, user facility, is supported by Laboratory Directed Research and Development (LDRD), Sandia National Laboratories. Sandia is a multiprogram laboratory operated by Sandia Corp., a Lockheed Martin Co., for the U.S. Department of Energy's National Nuclear Security Administration under Contract DE-AC04-94AL85000. The Materials Research Facilities Network (MRFN) program at the University of California, Santa Barbara, is funded by National Science Foundation grant DMR-0520415, for providing instrumentation support used to obtain materials characterization of samples.

References

1 N. S. Rogado, J. Li, A. W. Sleight and M. A. Subramanian, *Adv. Mater.*, 2005, **17**, 2225.
2 S. Zhao, L. Shi, S. Zhou, J. Zhao, H. Yang and Y. Guo, *J. Appl. Phys.*, 2009, **106**, 123901.
3 R. I. Dass and J. B. Goodenough, *Phys. Rev. B: Condens. Matter*, 2003, **67**, 014401.
4 R. N. Mahato, K. Sethupathi and V. Sankaranarayanan, *J. Appl. Phys.*, 2010, **107**, 09D714.
5 H. Das, U. V. Waghmare, T. Saha-Dasgupta and D. D. Sarma, *Phys. Rev. Lett.*, 2008, **100**, 186402.
6 S. Zhou, L. Shi, H. Yang and J. Zhao, *Appl. Phys. Lett.*, 2007, **91**, 172505.
7 M. P. Singh, S. Charpentier, K. D. Truong and P. Fournier, *Appl. Phys. Lett.*, 2007, **90**, 211915.
8 M. Sonobe and K. Asai, *J. Phys. Soc. Jpn.*, 1992, **61**, 4193.
9 M. C. Sánchez, J. García, J. Blasco, G. Subías and J. Pérez-Cacho, *Phys. Rev. B: Condens. Matter*, 2002, **65**, 144409.
10 C. L. Joseph, D. Gleeson and K. S. Knight, *J. Phys.: Condens. Matter*, 2003, **15**, 4927.
11 K. D. Truong, J. Laverdière, M. P. Singh, S. Jandl and P. Fournier, *Phys. Rev. B: Condens. Matter Mater. Phys.*, 2007, **76**, 132413.
12 M. P. Singh, K. D. Truong, J. Laverdière, S. Charpentier, S. Jandl and P. Fournier, *J. Appl. Phys.*, 2008, **103**, 07E315.
13 H. Z. Guo, A. Gupta, J. Zhang, M. Varela and S. J. Pennycook, *Appl. Phys. Lett.*, 2007, **91**, 202509.
14 P. A. Joy, Y. B. Khollam, S. N. Patole and S. K. Date, *Mater. Lett.*, 2000, **46**, 261.
15 H. Guo, A. Gupta, T. G. Calvarese and M. A. Subramanian, *Appl. Phys. Lett.*, 2007, **89**, 262503.
16 V. L. Joseph Joly, P. A. Joy and S. K. Date, *Phys. Rev. B: Condens. Matter*, 2002, **65**, 184416.
17 Y. Q. Lin and X. M. Chen, *J. Am. Ceram. Soc.*, 2011, **94**, 782.
18 I. Vrejoiu, M. Alexe, D. Hesse and U. Gösele, *Adv. Funct. Mater.*, 2008, **18**, 3892.
19 X. Zhu, Z. Liu and N. Ming, *J. Mater. Chem.*, 2010, **20**, 4015.
20 L. Ju, T. Sabergharesou, K. G. Stamplecoskie, M. Hegde, T. Wang, N. A. Combe, H. Wu and P. V. Radovanovic, *J. Am. Chem. Soc.*, 2012, **134**, 1136.
21 J. M. Schnorr and T. M. Swager, *Chem. Mater.*, 2011, **23**, 646.
22 H. Zhou, Y. Mao and S.S. Wong, *Chem. Mater.*, 2007, **19**, 5238.
23 Y. Mao, T.-J. Park, F. Zhang, H. Zhou and S.S. Wong, *Small*, 2007, **3**, 1122.
24 J. Burgess, H. Guo, A. Gupta and S. Street, *Vib. Spectrosc.*, 2008, **48**, 113.
25 *CRC Handbook of Chemistry and Physics*, Editor: R.C. Weast, 1st edn, CRC Press, Inc., Boca Raton, FL, 1988..

